Quantitative Relationship Between the Ratio of Fe^{2+}/Fe^{3+} in Fe_3O_4 and its Energy Gap in Photocatalytic Process

Shijie Zhang*

Hangzhou Synbest Biotech Co., Ltd, Hangzhou 311121, P.R. China.
zhsj123@aliyun.com*

Abstract: The energy gap of photocatalyst is important for photocatalytic processes. As a common substrate, the iron-based photocatalyst has attracted much attention due to its high catalytic activity. While, the basic functional relationship between the mole ratio of Fe^{2+}/Fe^{3+} in Fe_3O_4 nanoparticles (NPs) and the energy gap (Eg) is still unknown. this quantitative relationship was built by equations in this study. A series of experiments are carried out and the functional relationship is summarized by UV-Vis diffuse reflectance spectra (DRS) based on Kubelka-Munk theory. Meanwhile, its application for removing the organic dye Congo Red (CR) is examined. Optimum reaction conditions are obtained by orthogonal experiments. This study supplies a basic quantitative relationship between the ratio of Fe^{2+}/Fe^{3+} in Fe_3O_4 NPs and its energy gap. It is essential for designing all kinds of novel iron-based photocatalysts.

Keywords: Fe_3O_4, Photocatalysis, Quantitative relationship, Energy gap, Degradation, Congo Red.

Introduction

With the development of human society, people are confronted with the issue of environmental pollution resulting from the extensive utilization of fossil fuels.[1-3] To solve this problem, it is essential to develop non-polluting and sustainable energy supply systems. Solar power is a renewable resources. As an efficient and green catalyst, semiconductors can turn solar power into specific energy to drive various chemical reactions. [4-7] Among semiconductors, TiO_2 is a commercial photocatalyst and has been widely used due to its low cost, good ultraviolet (UV) absorption ability and low toxicity. [8-12] Different TiO_2-based photocatalysts have been developed, which have played a significant role in splitting water, the batteries manufacture and the removal of dyes, etc. [13] The use of TiO_2 in wastewater degradation has made great progress. [14] Recently, Ti–Fe oxide nanomaterials have been used to remove methyl orange dye in water. [15, 16] However, the wide energy gap (Eg = 3.2 eV) of TiO_2 leads to a weak response in visible spectrum (400 nm $< \lambda <$ 800 nm), [17-21] which restricts its application. In recent years, iron-based photocatalysts have received extensive attention due to their relative narrow band gaps and better responses in visible spectrum.[22-25] Abebe *et al*. also found that a Fe-oxide nanomaterial could remove pollutant because it has many adsorption sites, and it has a very good removal effect with maximum adsorption capacity of the adsorbent 70.422 mg/g. [26] Although iron-based photocatalysts have been widely studied, some fundamental questions still require explanation, such as the relationship between the mole ratio of Fe^{2+}/Fe^{3+} in Fe_3O_4 NPs and the Eg.

In continuous interest in photocatalysis, [27] iron-based photocatalysts have been successfully used for CO_2 fixation, [28] nitrogen fixation, [29] and degradation of dyes [30]. While the relationship between the mole ratio of Fe^{2+}/Fe^{3+} in Fe_3O_4 NPs and its Eg has not been reported. It is a fundamental problem in designing and preparing iron-based photocatalysts. Therefore, this research mainly explores this functional relationship, which can supply an accurate energy gap quantitative relationship for iron-based photocatalyst research. Meanwhile, the application of the photocatalyst for removing organic dyes in water was studied to provide a reference for iron-based photocatalyst application.

Experimental

Preparation of Fe_3O_4 NPs with different ratios of Fe^{2+}/Fe^{3+}

The Fe_3O_4 NPs with different mole ratios of Fe^{2+} and Fe^{3+} were synthesized via co-

---

*To whom all correspondence should be addressed.

precipitation using molysite in which Fe^{2+}/Fe^{3+} = 4.5:10. Based on the total concentration of molysite (0.30 mol·L^{-1}), the overall concentration ratios of Fe^{2+}/Fe^{3+} (34.5:10 (a), 25.5:10 (b), 14.5:10(c), 6.9:10(d), 4.5:10(e), 4.1:10(f), 2.9:10(g), 2.3:10(h)) were obtained by varying the amounts of $Fe_2SO_4·7H_2O$ and $FeCl_3$. The required amounts of Fe^{2+} and Fe^{3+} were dissolved in 6 mL of deionized water under argon. The above solutions were stirred for 20 min, followed by the addition of aqueous NaOH (0.25 mol·L^{-1}). The mixtures were then stirred for another 30 min at 60 ℃. The black suspensions were filtered, washed with water three times, and dried for 3 h at 100 ℃.

Catalytic activity measurements

5 mL of a CR aqueous solution (10 mg·L^{-1}) was added a defined amount of Fe_3O_4 NPs (a), (e), and (h). The above solutions were stirred at room temperature in dark for about 30 minutes until the adsorption-desorption reached equilibrium. Next, a 2.5 mL sample was taken from each solution at a predefined time (1 h and1.5 h). The suspensions were centrifuged (400 rpm, 7 min) and the absorbance of the suspensions were analysed by UV-vis spectrophotometry.

Results and Discussion

Fe_3O_4 NPs (a-h) with different ratios of Fe^{2+} and Fe^{3+} were prepared with concentration ratios of Fe^{2+} / Fe^{3+} as follows: 34.5:10 (a), 25.5:10 (b), 14.5:10(c), 6.9:10(d), 4.5:10(e), 4.1:10(f), 2.9:10(g), 2.3:10(h). The light collecting ability and the Eg value of these Fe_3O_4 NPs and their ability for the removal of Congo Red (CR) were then investigated.

Light-collecting ability

The light-collecting ability of catalysts can be tested by UV−Vis diffuse reflectance. The obtained curves for Fe_3O_4 NPs (a-h) had a strong light response in the range of 300-450 nm (Fig 1), which indicated that the Fe_3O_4 NPs had a good response performance in the visible region. Meanwhile, the Eg values of these samples were determined by UV-Vis diffuse reflectance spectra (DRS) based on Kubelka-Munk theory.
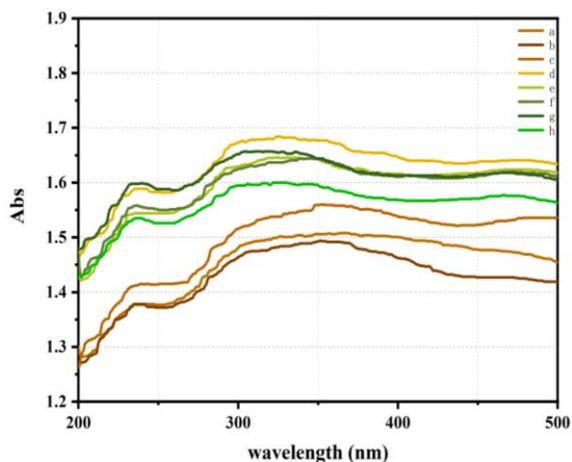

Fig 1:   UV−Vis diffuse reflectance spectra of Fe_3O_4 NPs with different mole ratios of Fe^{2+}/Fe^{3+}.

Calculation of Eg

Based on the information in Fig 1, the different band gap energies (Eg) can be obtained through equation (1) from Kubelka-Munk theory (Fig 2).[31,32]

$$(\alpha h\nu)^{n} = A(h\nu - Eg) \qquad (1)$$

where α is the absorption coefficient, h is Planck's constant, ν is the light frequency, and A is a constant. In particular, different types of optical transition semiconductors have a corresponding n value. That of a direct band gap semiconductor is 2 and that of an indirect band gap semiconductor is 1/2. So the n value is 1/2 for Fe_3O_4 NPs. The results are presented in Fig. 2
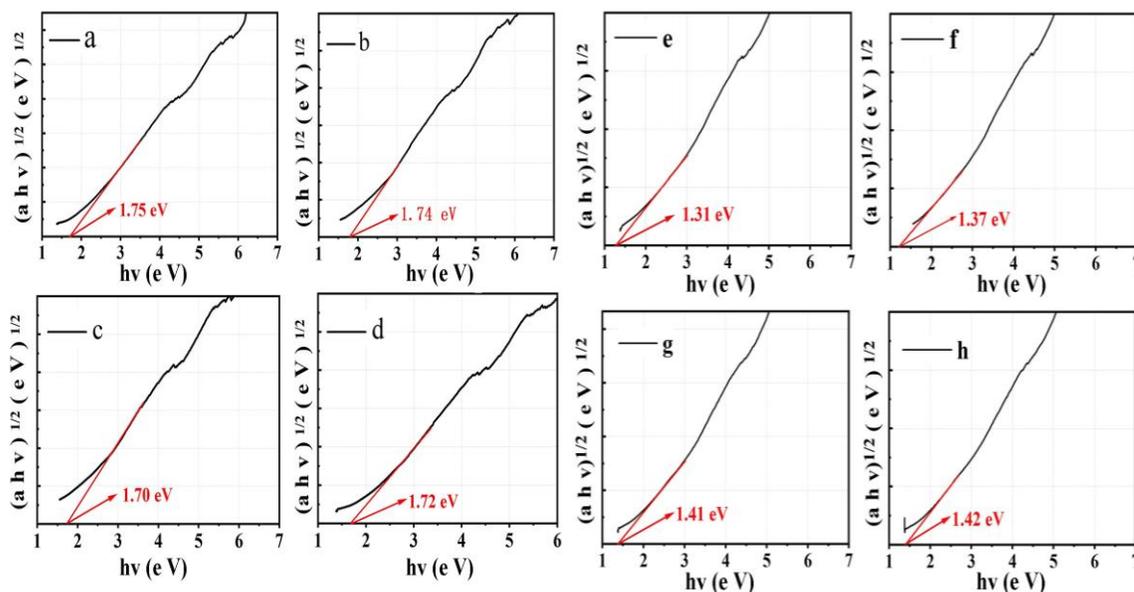
Fig. 2:   Band gap energies of Fe_3O_4 NPs with different mole ratios of Fe^{2+}/Fe^{3+}.

Equation fitting

To study the quantitative relationship between the Eg value and iron ion ratio in Fe_3O_4 NPs, their corresponding value was fitted with two applicable empirical equations. It was summarized in Fig 3 based on the above data.
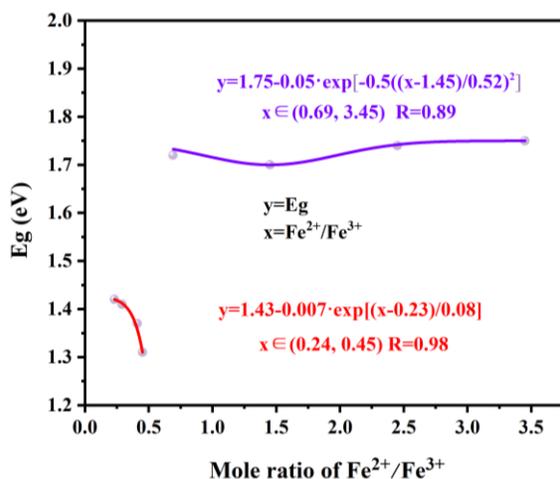

Fig. 3:   The relationship equations between the iron ion ratio and Eg value.

As shown in Fig 3, two equations were established by nonlinear fitting, where x is the concentration ratio of Fe^{2+}/Fe^{3+} (mol·L^{-1}), and y is

the Eg value. The R values reached 0.89 and 0.98, respectively, which shows that the two equations have good accuracy. Notably, this result indicated that a specific photocatalyst based on different iron ion ratios of Fe_3O_4 NPs could be designed and utilized in suitable light source.

$$y = 1.75 - 0.05 \cdot \exp[-0.5((x - 1.45)/0.52)^2] \ (2)$$

$$x \in (0.69, 3.45) \qquad R = 0.89$$

In the case of equation (2), with Fe^{2+} concentration increasing gradually, the Eg value decreased until the x value was 1.45 and the Eg value increased when x was greater than 1.45. According to equation (3), different absorption wavelengths were examined. The maximum absorption wavelengths of Fe_3O_4 NPs (a-d) were 708 nm, 712 nm, 730 nm, and 720 nm, respectively. This means that the energy in these wavelengths is the minimum energy required to activate electrons. So if researchers want to design a visible-response or ultraviolet-response iron-based photocatalyst, equation (2) could be employed to optimize the Fe_3O_4 NPs substrate.

In recent years, many photocatalysts based on iron substrate were designed and synthesized under the visible-response or

ultraviolet-response region. Wang *et al.* synthesized Fe_3O_4/BiOCl nanocomposites via a co-precipitation method, in which the Fe^{2+}/Fe^{3+} ratio $(mol \cdot L^{-1})$ is 1:1. This nanocomposite showed good photocatalytic activity toward RhB degradation in wavelength range of 200 to 800 nm.[33] Zhang *et al.* reported a Fe_3O_4@MIL-100(Fe) photocatalyst [Fe^{2+}/Fe^{3+} ratio $(mol \cdot L^{-1})$ is 1:1 in Fe_3O_4 NPs] that exhibited a 99% photocatalytic effect to MB degradation under the UV-vis or visible light irradiation.[34] The two photocatalysts based on iron showed a specific photocatalytic performance in visible or ultraviolet region. It is worth mentioning that these Fe^{2+}/Fe^{3+} ratios in Fe_3O_4 NPs match with equation (2) which shows that the fitting equation is credible.

$$Eg = 1240/n \qquad (3)$$

Equation (3), as mentioned in the previous paragraph, shows a relationship between the Eg value and the wavelength (n). [35] Hence, the absorption wavelengths from equations (2) and (4) can be examined using equation (3).

$$y = 1.43 - 0.007 \cdot exp[(x - 0.23)/0.08] \qquad (4)$$

$$x \in (0.24, 0.45) \qquad R = 0.98$$

In equation (4), the Eg value gradually increases with the Fe^{2+} concentration decreases. According to equation (3), the maximum absorption wavelengths of Fe_3O_4 NPs (e-h) are 946 nm, 905 nm, 879 nm, and 873 nm, respectively. This indicates that the energy in these wavelengths is the minimum energy required to activate electrons.

The difference with the above Fe_3O_4 NPs (a-d) is the different light response range. It has not only demonstrated visible and ultraviolet-responses, but a near-infrared (NIR)-response. Thus it has a wider light response range. In the past decade, due to the retrievability and the fact that the visible–NIR region occupies 95% of the total energy of the sunlight, photocatalysts based on Fe_3O_4 NPs have received wide attention.[35] They have much wider applications in infrared imaging, wastewater treatment, and removing organic dyes, etc.[36-38] According to equation (4), this studies indicated that photocatalysts based on iron could potentially be applied in the NIR region by adjusting the iron ratio in the Fe_3O_4 NPs.

Application for removing organic dyes

Fe_3O_4 NPs (a) were taken as an example to remove Congo Red (CR). It shows a removal rate of 98% for CR after sunlight irradiation for 1.5 h. As shown in Fig. 4 (a), CR shows a few changes after a dark reaction because it can reach adsorption equilibrium. After five recycling experiments, this catalyst still had good stability (Fig 4 b). Meanwhile, the removing CR experiment was performed under optimum reaction conditions, which were obtained by orthogonal experiments. The results are shown in Tables 1-3.
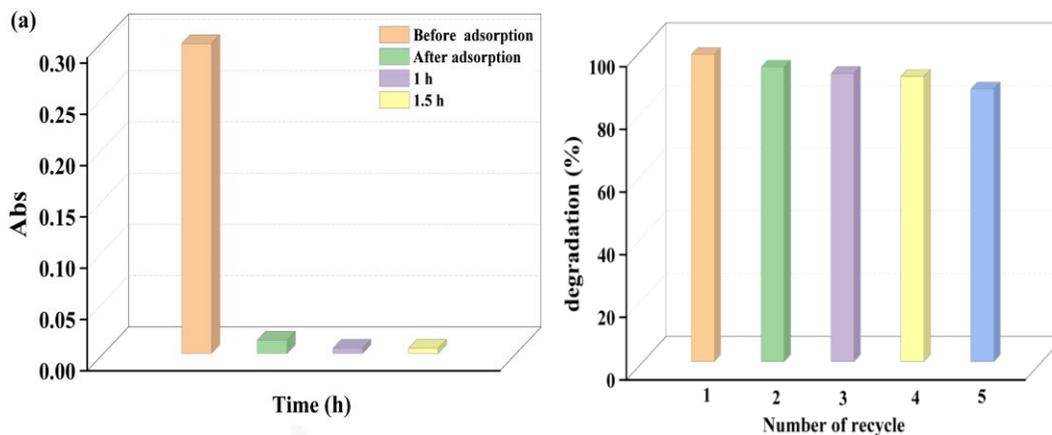
Fig. 4:   (a) Photocatalytic degradation of CR. (b) Catalyst recycling experiments.

Table-1: Orthogonal experimental design.

Entry	Time (h)	Congo Red (mg·L^{-1})	Cat. (mg)
a	0.5	10	5
b	1	15	10
c	1.5	20	15

Table-2: Orthogonal experimental results.

Entry	Time (h)	Congo Red (mg·L^{-1})	Cat. (mg)	Degradation rate (%)
1	0.5	10	5	93
2	0.5	15	10	86
3	0.5	20	15	97
4	1	10	10	90
5	1	15	15	94
6	1	20	5	64
7	1.5	10	15	96
8	1.5	15	5	89
9	1.5	20	10	97

Table-3: Analysis of the results.

Entry	Time (h)	Congo Red (mg·L^{-1})	Cat. (mg)
K1	92	93	82
K2	83	90	91
K3	94	86	96
R	11	7	14

The reaction conditions for CR degradation were optimized via orthogonal experiments. Table 1 presents three factors and levels namely reaction time (0.5 h, 1 h, 1.5 h), substrate concentration (10 mg·L^{-1}, 15 mg·L^{-1}, 20 mg·L^{-1}) and catalyst amount (5 mg, 10 mg, 15 mg). The results in Table 2 show the degradation rate of CR under different experimental conditions. Then, the optimum experimental conditions are obtained by the K (K1, K2, K3) and R value in Table 3, which are calculated based on the results in Table 2. The maximum K value in a single factor represents the best reaction conditions under this factor.

In Table 3, the maximum K value in factors reaction time, substrate concentration, and catalyst amount are K3 (94), K1 (93), and K3(96), respectively. Therefore, the optimum experimental conditions are reaction time (1.5 h), substrate concentration (10 mg·L^{-1}), and catalyst amount (15 mg). Meanwhile, the maximal R value represents it is the most important factor among all factors. So the maximum R value is 14 in Table 3, which represents the catalyst amount is the foremost factor in CR degradation.

Exploration of possible mechanisms

Compared with this result, Yirga *et al*. studied the effects of different conditions influence on the adsorption of methylene blue (MB) by Fe$_3$O$_4$ NPs. [39] The plentiful vacant surface sites become occupied by dye molecules until the system reaches adsorption-desorption equilibrium. In this study, after optimizing, 1.5 h is suitable for reaching the adsorption equilibrium. Basically, the catalysts with a larger ratio of active adsorption sites show better adsorption performance. In this work, it shows a good absorption efficiency at the lowest substrate concentration (10 mg·L^{-1}), which indicates that the catalyst has a high adsorption site ratio. Therefore, the number of vacant surface sites increases as the amount of catalyst increases. Based on the optimized conditions, CR was removed using three different mole ratios of Fe$_3$O$_4$ NPs (34.5:10(a); 4.5:10(e), 2.3:10(h)). The results show that Fe$_3$O$_4$ NPs (a) with a maximum Eg value has a 98% degradation ratio. The Fe$_3$O$_4$ NPs (e) with a minimum Eg value has a 70% degradation ratio (Fig 5). So the energy gap has an impact on the catalytic degradation of organic dyes.
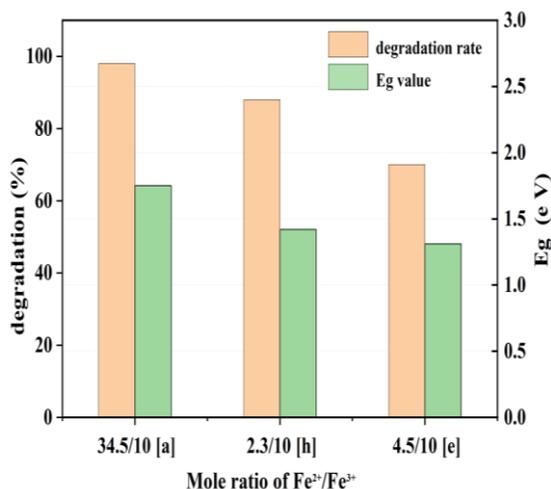
Fig. 5:   The CR degradation ratios using different mole ratios of Fe^{2+}/Fe^{3+}.

Different nano-morphology

The nanostructures of Fe_3O_4 NPs (a, e) are shown in Fig 6. For Fe_3O_4 NPs (a, 3.45:10) and (e, 4.5:10), the diameter of the nanoparticle (a) is about 66 nm, being smaller than that of nanoparticles (e) at 75 nm. According to the co-precipitation method, an increasing Fe^{2+} concentration may restrain the reverse reaction, which could generate more Fe_3O_4 NPs. However, more nanoparticles could increase agglomeration.
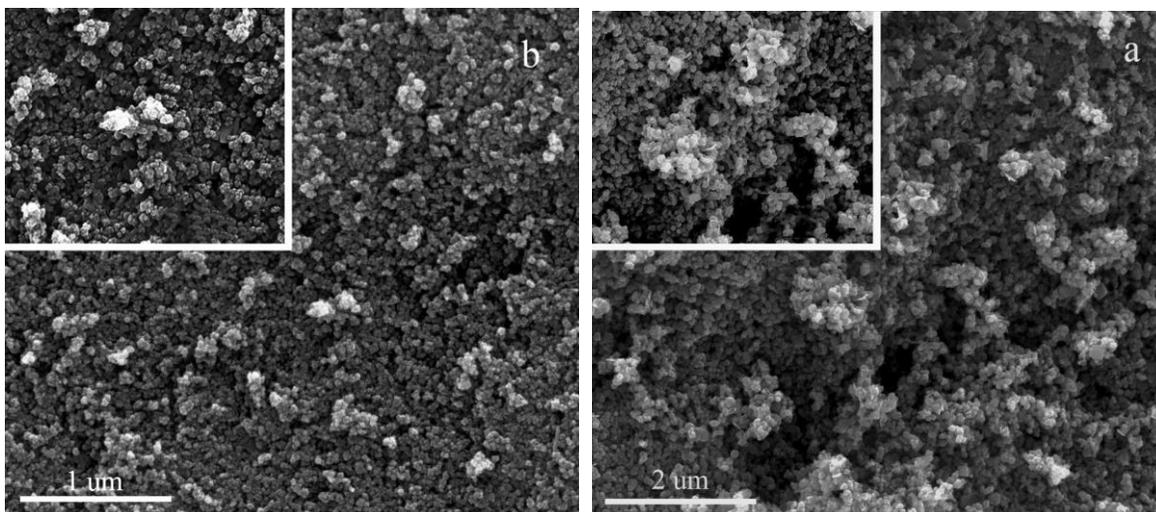
So Fe_3O_4 NPs (a) form larger lumps than Fe_3O_4 NPs (e) according to SEM. This result means that more Fe_3O_4 NPs may adsorb more dye molecules for a greater contact area, thus leading to good performance for removing organic dyes.

XRD

As shown in Fig 7, the synthetic Fe_3O_4 NPs (a, 34.5:10), employed to remove CR were examined by XRD. The results agree with the cubic phases of Fe_3O_4 NPs. The 2θ and Miller indices of $30.1°(220)$, $35.5°(311)$, $43.1°(400)$, $57.1°(511)$, and $62.7°(440)$ matched with reference code: 01-088-0315.

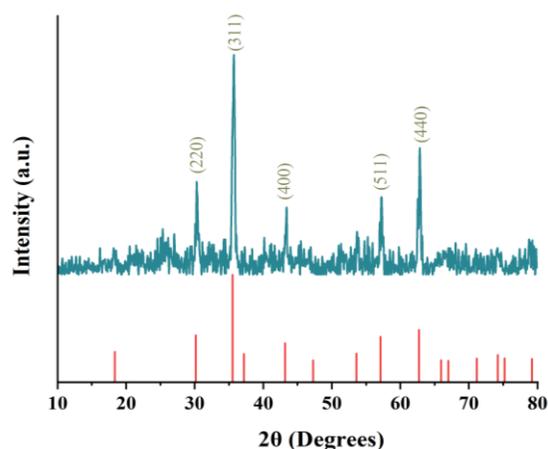Fig. 7:   XRD of Fe_3O_4 NPs (a, 34.5:10).

Fig. 6:   SEM images of Fe_3O_4 NPs (a, 34.5:10) and natural Fe_3O_4 NPs (b, 4.5:10).

Conclusion

In summary, the quantitative relationship between the mole ratio of Fe^{2+}/Fe^{3+} in Fe_3O_4 and the energy gap has been investigated fully by UV−Vis diffuse reflectance based on Kubelka-Munk theory. This quantitative relationship was successfully built by equations. This work studies a light-response region for the photocatalyst based on Fe_3O_4 NPs and it can supply a f undamental data for designing all kinds of iron-based photocatalysts in catalytic field. Its photo-degradation properies for CR indicate this ratio of Fe^{2+}/Fe^3 regulation in Fe_3O_4 can influence its photocatalytic ability. The experimental results proves that the quantitative relationship equations is reliable for designing iron-based photocatalyst.

Reference

1. H. Tong, S. X. Ouyang, Y. P. Bi, N. Umezawa, M. Oshikiri, and J. H. Ye, Nano-photocatalytic materials: possibilities and challenges, *Adv. Mater*. **24**, 229 (2012).

2. Z. Fu, Q. Yang, Z. Liu, F. Chen, F. Yao, T. Xie, Y. Zhong, D. Wang, J. Li, X. Li and G. Zeng, Photocatalytic conversion of carbon dioxide: from products to design the catalysts, *J CO2 Util*. **34**, 63 (2019).

3. X. Li, W. Bi, Z. Wang, W. Zhu, W. Chu, C. Wu and Y. Xie, Surface-adsorbed ions on TiO_2 nanosheets for selective photocatalytic CO_2 reduction, *Nano Res*. **11**, 3362 (2018).

4. S. M. Gupta and M. Tripathi, A review of TiO_2 nanoparticles, *Chin Sci Bull*. **56**, 1639 (2011).

5. D. M. Schultz and T. P. Yoon, Solar synthesis: prospects in visible light photocatalysis, *Sci*. **343**, 6174 (2014).

6. C. P. Sajan, S. Wageh, A. A. Al-Ghamdi, J. Yu and S. Cao, TiO_2 nanosheets with exposed {001} facets for photocatalytic applications, *Nano Res*. **9**, 3 (2015).

7. J. Zhang, W. Hu, S. Cao and L. Piao, Recent progress for hydrogen production by photocatalytic natural or simulated seawater splitting, *Nano Res*. **13**, 2313 (2020).

8. U. I. Gaya and A. H. Abdullah, Heterogeneous photocatalytic degradation of organic contaminants over titanium dioxide: a review of fundamentals, progress and problems, *J Photochem Photobiol C: Photochem Rev*. **9**, 1 (2008).

9. M. Dahl, Y. Liu and Y. Yin, Composite titanium dioxide nanomaterials, *Chem Rev*. **114**, 9853 (2014).

10. D. P. Agatino, B. Marianna and P. Leonardo, Brookite, the least known TiO_2 photocatalyst, *Catalysts*. **3**, 36 (2013).

11. R. Leary and A. Westwood, Carbonaceous nanomaterials for the enhancement of TiO_2 photocatalysis, *Carbon*. **49**, 741 (2011).

12. Q. Li, H. Kong, R. Jia, J. Shao and Y. He, Enhanced catalytic degradation of amoxicillin with TiO_2–Fe_3O_4 composites via a submerged magnetic separation membrane photocatalytic reactor (smsmpr), *RSC Adv*. **9**, 12538 (2019).

13. M. R. Kumar, B. Abebe, H. P. Nagaswarupa, H. C. Murthy, C. R. Ravikumar and F. K. Sabir, Enhanced photocatalytic and electrochemical performance of TiO_2-Fe_2O_3 nanocomposite: its applications in dye decolorization and as supercapacitors, *Sci Rep*. **10**, 1249 (2020).

14. B. Abebe, H. C. A. Murthy and E. Amare, Summary on adsorption and photocatalysis for pollutant remediation: mini review, *Encapsulation Adsorpt Sci*. **8**, 225 (2018).

15. B. Abebe, H. C. A. Murthy and Y. Dessie, Synthesis and characterization of Ti–Fe oxide nanomaterials: adsorption–degradation of methyl orange dye, *Ara Sci Eng*. **45**, 4609 (2020).

16. B. Abebe and H. C. A. Murthy, Synthesis and characterization of Ti-Fe oxide nanomaterials for lead removal, *J Nanomater*. **2018**, 1 (2018).

17. V. Etacheri, C. D. Valentin, J. Schneider, D. Bahnemann and S. C. Pillai, Visible-light activation of TiO_2 photocatalysts: advances in theory and experiments, *J Photochem Photobio C, Photochem Rev*. **25**, 1 (2015).

18. M. N. Chong, B. Jin, C. W. K. Chow and C. Saint, Recent developments in photocatalytic water treatment technology: a review, *Water Res*. **44**, 2997 (2010).

19. M. D. Hernández-Alonso, F. Fresno, S. Suárez and J. M. Coronado, Development of alternative photocatalysts to TiO_2: challenges and opportunities, *Energy Environ Sci*. **2**, 1231 (2009).

20. W. Wang, K. Xiao, L. Zhu, Y. Yin and Z. Wang, Graphene oxide supported titanium dioxide & ferroferric oxide hybrid, a magnetically separable photocatalyst with enhanced photocatalytic activity for tetracycline hydrochloride degradation, *RSC Adv*. **7**, 21287 (2017).

21. C. Fu, X. Liu, Y. Wang, L. Li and Z. Zhang, Preparation and characterization of

Fe_3O_4@SiO_2@TiO_2–Co/rGO magnetic visible light photocatalyst for water treatment, *RSC Adv.* **9**, 20256 (2019).

22. S. Natarajan, K. Harini, G. P. Gajula, B. Sarmento, M. T. Neves-Petersen and V. Thiagarajan, Multifunctional magnetic iron oxide nanoparticles: diverse synthetic approaches, surface modifications, cytotoxicity towards biomedical and industrial applications, *BMC Mat.* **1**, 2 (2019).

23. L. Xie, Z. Yang, W. Xiong, Y. Zhou, J. Cao, Y. Peng, X. Li, C. Zhou, R. Xu and Y. Zhang, Construction of MIL-53(Fe) metal-organic framework modified by silver phosphate nanoparticles as a novel Z-scheme photocatalyst: visible-light photocatalytic performance and mechanism investigation, *Appl Surf Sci.* **465**, 103 (2019).

24. L. Tang, Z. Lv, Y. Xue, L. Xu, W. Qiu, C. Zheng, W. Chen and M. Wu, MIL-53(Fe) incorporated in the lamellar BiOBr: Promoting the visible-light catalytic capability on the degradation of rhodamine B and carbamazepine, *Chem Eng J.* **374**, 975 (2019).

25. M. Ahmad, S. Chen, F. Ye, X. Quan, S. Afzal, H. Yu and X. Zhao, Efficient photo-Fenton activity in mesoporous MIL-100(Fe) decorated with ZnO nanosphere for pollutants degradation, *Appl Catal B-Environ.* **245**, 428 (2019).

26. B. Abebe and H. C. A. Murthy, Fe-oxide nanomaterial: synthesis, characterization and lead removal, *Encapsulation Adsorpt Sci.* **8**, 195 (2018).

27. S. Yang, Q. Sun, Y. Shen, Y. Hong, X. Tu, Y. Chen and H. Zheng, Design, synthesis and application of new iron-based cockscomb-like photocatalyst for high effectively degrading water contaminant under sunlight, *Appl Surf Sci.* **525**, 13 (2020).

28. X. Tu, Y. Chen, C. Sun, Y. Hu, S. Zhu, J. Qu, Z. Zhu, S. Zhang and H. Zheng, A novel CO_2 fixation catalyst FCO@NWs to synthesize benzimidazole at atmospheric pressure, *J Environmental Chemical Engineering.* **12**, 112097 (2024).

29. C. Sun, S. Zhu, J. Qu, Z. Zhu, Y. Chen, X. Tu, W. Cai, Z. Yu, Y. Liu, S. Zhang and H. Zheng, Efficient photocatalytic nitrogen fixation via oxygen vacancies in Zr-MOFs at ambient conditions, J Colloid and Interface Science669, 75-82 (2024).

30. Weihang Han, Jingxuan Shou, Yifan Yang, Liangchen Chen, Luping Zhang, Yutong Chen, Xuewei Tu, Dan Jin, Shijie Zhang, Yurong Chang, Hui Zheng, High efficient removal of tetracycline in water via porous magnetic Ce/Fe photocomposite under visible light. *Journal of Rare Earth.* **41**, 1532-1540 (2023).

31. J. Zheng and L. Zhang, Designing 3D magnetic peony flower-like cobalt oxides/g-C_3N_4 dual Z-scheme photocatalyst for remarkably enhanced sunlight driven photocatalytic redox activity, *Chem Eng J.* **369**, 947 (2019).

32. H. He, J. Cao, M. Guo, H. Lin, J. Zhang, Y. Chen and S. Chen, Distinctive ternary CdS/Ni_2P/g-C_3N_4 composite for overall water splitting: Ni_2P accelerating separation of photocarriers, *App Catal B: Environ.* **249**, 246 (2019).

33. W. Wang, M. He, H. Zhang and Y. Dai, Facile synthesis of flower-like superparamagnetic Fe_3O_4/BiOCl nanocomposites as high effective magnetic recyclable photocatalyst under visible light, *J Magn.* **21**, 179 (2016).

34. C. Zhang, L. Qiu, F. Ke, Y. Zhu, Y. Yuan, G. Xu and X. Jiang, A novel magnetic recyclable photocatalyst based on a core–shell metal–organic framework Fe_3O_4@MIL-100(Fe) for the decolorization of methylene blue dye, *J Mater Chem A.* **1**, 14329 (2013).

35. J. Zhang, W. Hu, J. Zhang, S. Liu, J. Tong, X. Hou, W. Liu, J. Yang and B. Liu, Stable heteropolyoxotitanate nanocluster for full solar spectrum photocatalytic hydrogen evolution, *J Phys Chem C.* **121**, 18326 (2017).

36. S. Huang, Z. Lou, N. Zhu, A. Shan and L. Li, Preparation of CaF_2/TiO_2/$Ln_2Ti_2O_7$ (Ln = Er, Tm, Yb) based magnetite near-infrared photocatalyst supported on waste ferrite, *Mater Res Bull.* **86**, 107 (2017).

37. S. Huang, H. Wang, N. Zhu, Z. Lou, L. Li, A. Shan and H. Yuan, Metal recovery based magnetite near-infrared photocatalyst with broadband spectrum utilization property, *Appl Catal B: Environ.* **181**, 456 (2016).

38. M. Humayun, A. Zada, Z. Li, M. Xie, X. Zhang, Y. Qu, F. Raziq and L. Jing, Enhanced visible-light activities of porous $BiFeO_3$ by coupling with nanocrystalline TiO_2 and mechanism, *Appl Catal B: Environ.* **180**, 219 (2016).

39. G. Yirga, C. Murthy and B. H. Eshetu, Synthesis and characterization of humic acid-coated Fe_3O_4 nanoparticles for methylene blue adsorption activity, *Adv Mater Lett.* **10**, 715 (2019).